J. Micromech. Microeng. **18** (2008) 075033 (9pp) doi:10.1088/0960-1317/18/7/075033

An improved in-plane thermal folded V-beam actuator for optical fibre alignment

W P Sassen[1], V A Henneken[1], M Tichem[1] and P M Sarro[2]

[1] Laboratory for Micro and Nano Engineering, Delft University of Technology, Mekelweg 2, 2628 CD Delft, The Netherlands
[2] Delft Institute of Microsystems and Nanoelectronics (DIMES), Delft University of Technology, Feldmannweg 17, 2628 CT Delft, The Netherlands

E-mail: m.tichem@tudelft.nl

Received 11 January 2008, in final form 28 May 2008
Published 19 June 2008
Online at stacks.iop.org/JMM/18/075033

Abstract
This paper presents an improved thermal actuator design, providing high work per unit of chip area. The actuator was developed for high accuracy fibre alignment. This application requires that the fibre tip is moved by pushing close to its end, posing geometric design constraints on the actuator design. The basic structure of the actuator is a parallelogram, consisting of a non-moving base, a bar parallel to the base placed orthogonal to the fibre axis in contact with the fibre, and heater arms and reinforced restraining arms which connect the base and the bar. The heater arms thermally expand when passing a current through them. On either side of the heater arms there is one restraining arm, placed at a slightly different angle with the base and bar than the heater arms. The restraining arms do not heat up, and constrain the motion due to thermal expansion of the heater arms, resulting in a motion of the bar in its longitudinal direction. The performance of this actuator is compared to two well-known alternative thermal actuator configurations. Comparison shows that the improved actuator delivers 15% more work per area, and is therefore considered an attractive alternative solution for purposes such as in-plane optical fibre alignment.

(Some figures in this article are in colour only in the electronic version)

1. Introduction

Optical fibre alignment tasks are technologically challenging due to the high-accuracy alignment involved. The required positioning accuracy for the fibre tip with respect to the laser diode is approximately $\pm$ 0.1 μm, whereas the required actuation stroke is typically in the order of tens of micrometres, and the required force in the milli-Newton range.

Thermal actuators are highly suitable for performing fibre alignment tasks because of their ability to deliver large forces in combination with large actuator displacements. MEMS-based thermal actuators can be found in several shapes and configurations. For the alignment of an optical fibre to a laser diode, a design which has a single-ended arrangement is preferred since it enables clear access to the fibre tip. Also a small chip area is desired to reduce fabrication costs. Therefore, actuator configurations capable of delivering a sufficiently large amount of work on the smallest possible chip area are much in demand.

Several options for the single-ended design exist, but they have been discarded as they are not good candidates for the design problem at hand. For instance, the well-known U-beam actuator [1, 2], although it has a single-ended design, is not suitable because of its low stiffness in lateral direction. Achieving a large fibre displacement would therefore require a very large actuator, which is not preferred. Although placing U-beam actuators in parallel increases the stiffness, this also lowers the actuator efficiency because of significant internal stress build-up and unwanted heat flow by conduction from the hot arms towards the cold arms. Kopka *et al* [3] have presented an arrangement of two series-connected bulk-micromachined actuators, in which the current flow can be directed through

 © 2008 IOP Publishing Ltd Printed in the UK

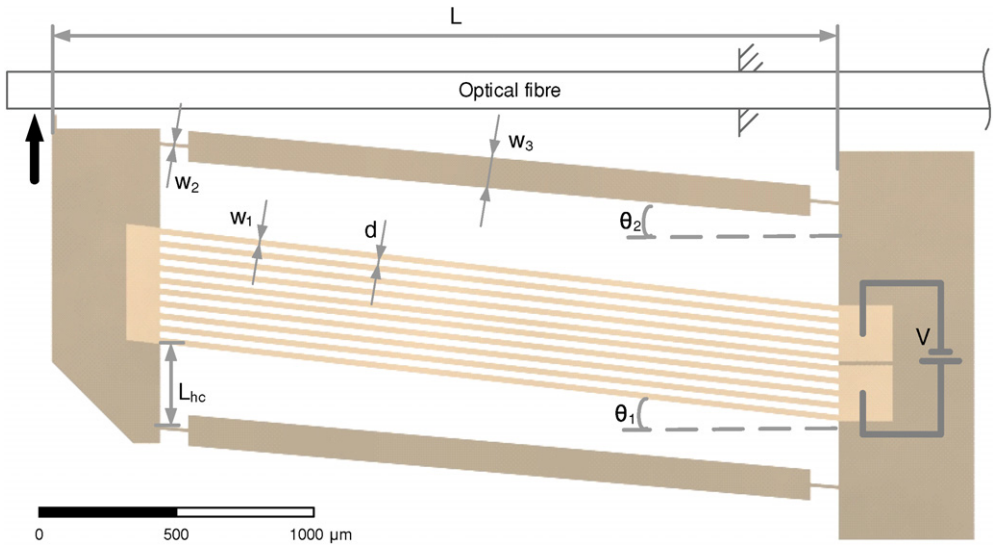


Figure 1. The layout of the folded V-beam actuator geometry for lateral fibre tip displacement: the device has ten hot actuation arms and two reinforced cold restraining arms.

a linking bridge. This concept is difficult to fabricate and therefore not further considered. A conventional buckling mode or V-beam actuator (e.g. [4]) could also be used for fibre alignment purposes. However, without any adaptations, a clear access to the fibre tip is not possible. With some adjustments to the design of the V-beam concept, such as by using a compliant lever, it can be made more suitable for fibre positioning.

An alternative in-plane thermal actuator design intended for single-ended fibre tip manipulation was presented by Syms *et al* [5]. The design was effectively a folded, multiple element V-beam actuator, of which the single-ended design allowed clear access to the fibre tip. Quite promising initial results were achieved using this novel folded V-beam actuator configuration.

In this paper, an improved design of this actuator is presented and compared to the two conventional V-beam actuator configurations including levers to obtain the same clear fibre tip access. The design and working principle of the improved actuator and of the alternative actuator configurations is introduced. Details of fabrication and measurement results are given. The electrical, thermal and mechanical modelling of the improved actuator design is discussed and its performance compared to the other configurations.

2. Design

The folded V-beam actuator (see figure 1) has an array of 'hot' actuation arms which will resistively heat up when a voltage is applied. The thermal expansion in axial direction caused by the heating is converted into a motion nearly perpendicular to the fibre axis by two additional 'cold' restraining arms that are placed at a smaller angle to the fibre axis than the hot arms. The restraining arms do not carry any electrical current and are connected to the actuator arms by a stiff link bar. The voltage is applied to the hot arms which are grouped in two sets that are serially connected.

Based on finite element (FE) modelling, the actuator dimensions are determined. The concept uses ten actuation arms with a uniform width w_1 of 25 μm placed at a spacing d of 20 μm and two reinforced restraining arms of which the narrow parts are 15 μm wide and 125 μm long. The reinforced segments have a width w_3 of 75 μm. The hot arm angle θ_1 and cold arm angle θ_2 are 7° and 5°, respectively, resulting in an angle difference between the hot arms and the cold arms of 2°. The distance between the hot arms and the cold arms is described by the length L_{hc} that equals 300 μm and the overall length of the concept, L, is 3000 μm.

Compared to the original design as presented by Syms *et al* [5], modifications were made on the actuator fabrication and on its geometry, similar to the improvements recently made by Veladi *et al* [6]. The fabricational and geometrical improvements are treated here separately.

For the fabrication, Syms *et al* used a silicon-on-insulator (SOI) wafer, in which the structures are released by etching the 2 μm thick buried oxide layer. The resulting small air gap caused significant heat loss towards the underlying substrate. To reduce heat loss, we have manufactured freestanding structures in the bulk material of a standard silicon wafer. The structure thickness was increased from 85 μm to 150 μm to enhance its robustness, and polysilicon was used for heating, instead of chrome and gold, thereby allowing higher actuation temperatures.

The main geometry modifications are performed on the restraining arms. Ideally, perfectly isolated restraining arms would be needed for an optimal performance of the actuator. In practice, heat flows from the actuator arms into the cold arms via the link bar. In order to lower the temperature rise from heat flowing in the cold arms, the original cold arms are replaced by reinforced restraining arms that have an increased heat-removing capability. Additionally, their stiffness in the motion direction is low, but high in the longitudinal direction,

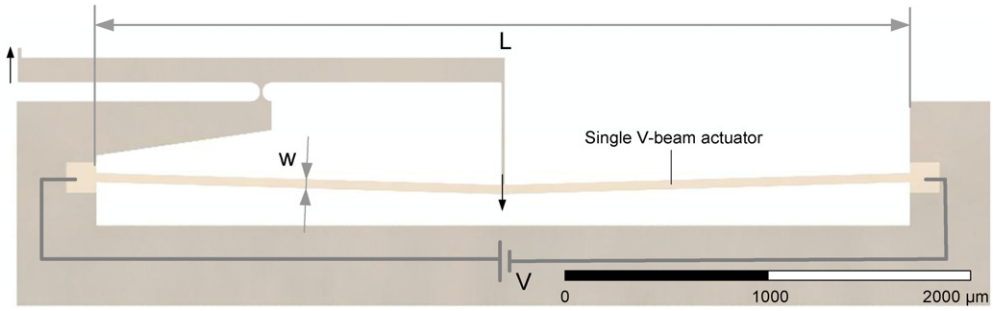


Figure 2. Single V-beam actuator design including lever with a 1:1 transmission ratio.

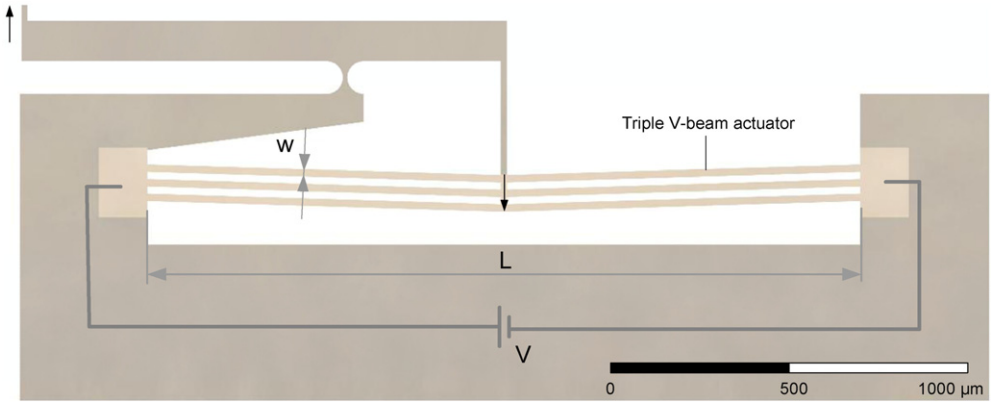


Figure 3. Triple V-beam actuator design including lever with a 1:2 transmission ratio.

resulting in low mechanical resistance against actuation, while maximally restraining the hot arms in order to convert their elongation as much as possible into a lateral actuator motion.

Besides by conduction via the link bar, the restraining arms are also heated by conduction through air. Therefore, the distance between the actuator arms and the restraining arms is increased. This requires a stiffer link bar between the hot and cold arms, and thus its width has been increased.

According to the results obtained by Syms *et al*, the actuators perform well in case an angle difference between the hot and cold arms of between 0.5° and 3° is used. We set the angle difference to 2°, and increased angles θ_1 and θ_2. Based on the kinematics of the structure the movement is theoretically circular; however, the 'cold' restraining arms expand a certain amount due to heating, causing the end effecter to follow approximately a straight line perpendicular to the fibre axis.

The performance of the improved folded V-beam actuator is then compared to that of two V-beam concepts including levers (see figures 2 and 3), one with a single V-beam actuator and one with a triple V-beam actuator, and having a 1:1 and a 1:2 transmission ratio, respectively. They were dimensioned in such a way that all three concepts are expected to achieve approximately similar performances.

The single V-beam concept layout is shown in figure 2. The substrate on the left side is required to keep the left V-beam anchor in position when actuating. It is therefore also part of the design. The V-beam actuator is 4000 μm long and 50 μm wide with an angle of 1.72° (0.03 rad). The lever has a length of 2400 μm and is mounted exactly halfway on a flexure hinge having a radius of 50 μm and a minimal width of 15 μm, which acts as an almost ideal pivot.

The third concept uses a triple V-beam stack which is much smaller than the single V-beam actuator and therefore also delivers a smaller displacement. In order to achieve the required displacement at the lever tip a lever with a 1:2 transmission ratio is used to amplify the actuator motion by a factor of 2. The extra V-beams in the actuator stack are necessary to deliver the required force. The actuator beams are 2000 μm long and 25 μm wide and are also manufactured with a 1.72° angle. The lever is mounted at one third of its total length (1500 μm) on a flexure hinge with the same dimensions as the flexure hinge in the single V-beam concept. The triple V-beam actuator concept is presented in figure 3.

The three different concepts all require a comparable chip area (∼4–6 mm^2, see table 1 in section 6). All concepts are manufactured using the fabrication sequence described in the following section.

3. Fabrication

The positioning of the optical fibre requires relatively large forces and a robust design of the structures. For this reason, the structures are manufactured in a standard 525 μm thick silicon wafer. In this wafer a 150 μm thick membrane is created by anisotropic etching in a KOH solution from the backside of the wafer. The structures are then defined in the membrane by deep reactive ion etching (DRIE) from the front side. Heating of the thermal actuators in the device takes

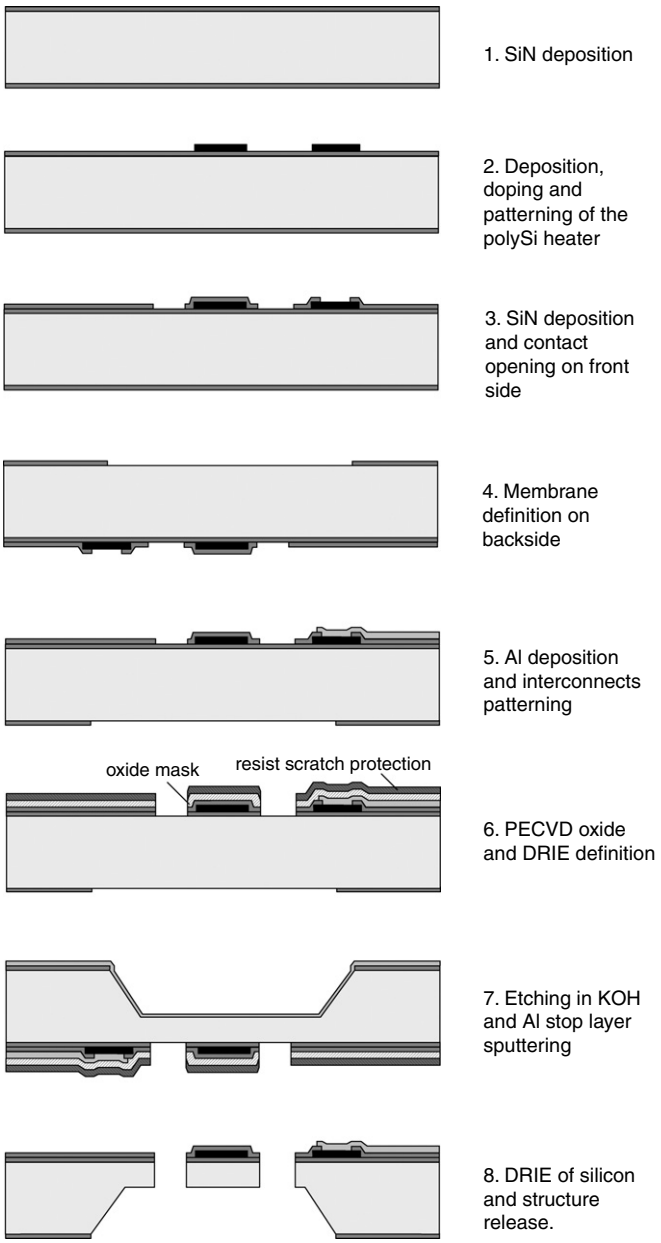


Figure 4. Fabrication sequence of the in-plane actuation structures.

place by current flow through a thin polysilicon layer on top of the bulk material. The fabrication sequence, which globally consists of eight steps, is schematically presented in figure 4.

A 300 nm thick low stress SiN layer (figure 4(*a*)), followed by a 500 nm thick low stress polysilicon layer, is deposited by LPCVD. The polysilicon layer is doped with phosphorous using a diffusion process and patterned using a resist mask and a dry etching step (figure 4(*b*)). The final resistivity of the layer is 19.5 Ω sq. Next, a second SiN layer is deposited on the polysilicon and patterned to form contact openings to the polysilicon (figure 4(*c*)). The membranes on the backside of the wafer are then defined by dry etching of the SiN layer (figure 4(*d*)).

At this point the aluminium metallization is realized (figure 4(*e*)), followed by the deposition and patterning of a 3.0 μm thick PECVD oxide layer to be used as a mask during the 150 μm deep silicon etch to release the beams (figure 4(*f*)). Before the DRIE step the membranes are formed by wet anisotropic etching of silicon from the backside in a 33wt% KOH solution at 85 °C. The etching process is stopped once a 150 μm thick silicon membrane remains (figure 4(*g*)). A 500 nm aluminium stop layer for the DRIE process is then deposited in the etched cavities and the DRIE etch is performed from the front side. Finally, the remaining oxide on the front side and the aluminium stop layer are removed to release the structure (figure 4(*h*)).

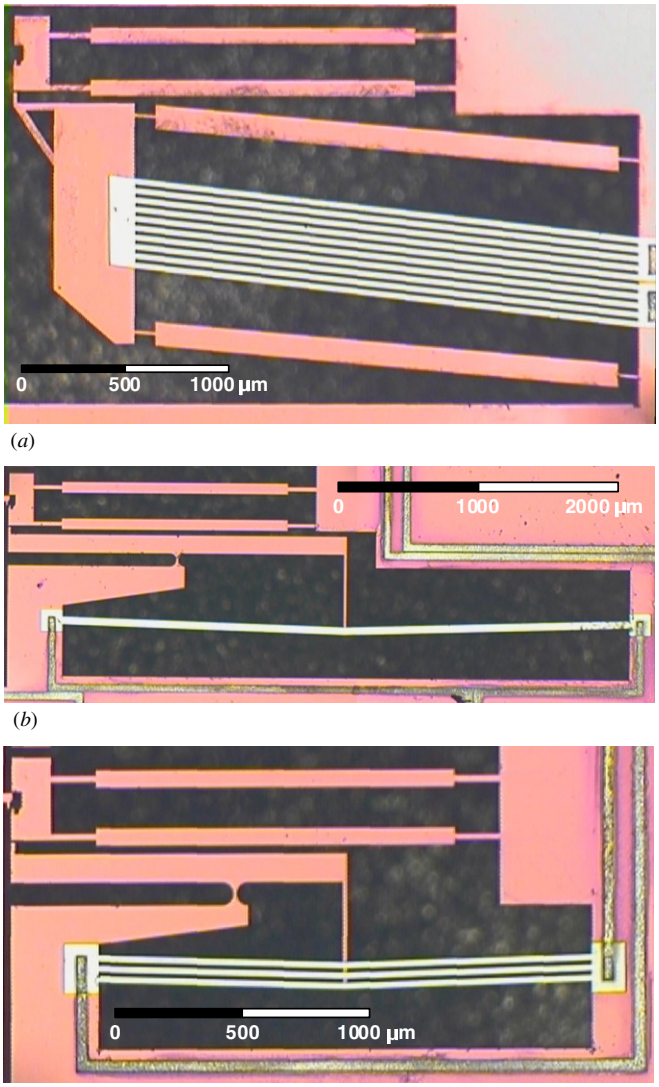
Figure 5 shows overview images of the fabricated actuator devices. On the top half of each image a mechanism is shown which is created to simulate the passive fibre force on the actuator device. It was given a lateral stiffness (200 N m^{-1}) comparable to a 2500 μm long single side clamped fibre end. Due to a 10 μm fabrication gap between the actuator tip and the mechanism, the actuator has a free displacement of 10 μm before the opposing force on the actuator starts to build up. The results presented in this paper are all related to measurements including such a fibre mechanism.

4. Results

The steady-state and transient actuator behaviour of the individual concepts is investigated by measuring the displacement, the step response and ring down behaviour. The step response and ring down behaviour describe the time behaviour of the output displacement upon an input voltage change from zero to a certain nonzero value in a very short time, and vice versa. These measurements are performed using the in-plane functionality of a Polytec laser vibrometer, which uses repetitive pattern recognition to determine the actuator displacement as a function of time or voltage with an accuracy of around 50 nm.

Before investigating the steady-state and transient behaviour of the individual actuators, for each actuator the maximum allowable voltage is determined. Above a temperature of approximately 870 K the heater elements started to exhibit resistance changes due to recrystallization of the polysilicon, possibly followed by thermal runaway [7, 8]. Although actuation up to temperatures at which these changes just started to take place did not lead to noticeable damage, a maximum temperature of around 770 K, that is 100 degrees lower than the polysilicon recrystallization temperature, was taken for safety. It was shown that this type of actuators can be operated for several millions of actuation cycles at this temperature [4]. During the experiments the actuators are all loaded up to 34 V, which is below the maximum allowable voltage. The actual maximum voltage is determined afterwards using finite element modelling of which the results are presented in the next section.

The measured displacements as a function of input voltage are presented in figure 6. The displacements of the single V-beam actuator and the folded V-beam actuator are almost equal over the full voltage range. The concept using a triple V-beam actuator showed a significantly higher deflection at the same input voltage level.



(*a*)

(*b*)

(*c*)

Figure 5. Overview image of (*a*) the improved folded V-beam actuator, (*b*) the single V-beam actuator and (*c*) the triple V-beam actuator, all including the passive mechanism representing the stiffness of an optical fibre.

The displacements as function of input power are shown in figure 7. Coincidentally, the triple V-beam actuator and the folded V-beam actuator required almost exactly the same amount of power to achieve a certain displacement.

The main heat loss mechanism for the actuators is conduction through the solid actuator. Due to the length of the single V-beam actuator compared to its width, less heat is dissipated than with the other two actuators. The single V-beam actuator, therefore, has a higher efficiency and requires less power to achieve the same displacement as the other two concepts.

At 34 V, the triple V-beam actuator reached significantly higher deflections than the other two actuators; however, it cannot be loaded much further, whereas the single V-beam actuator and the folded V-beam actuator can be loaded to higher voltages, as indicated in table 1.

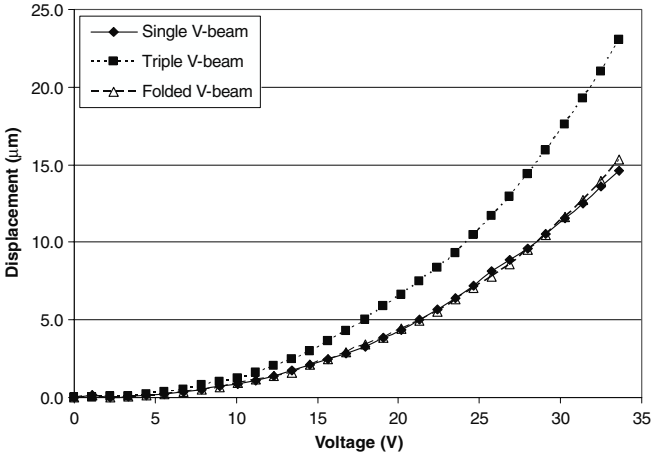


Figure 6. Experimental voltage-displacement curves 0–34 V including passive mechanism loading.

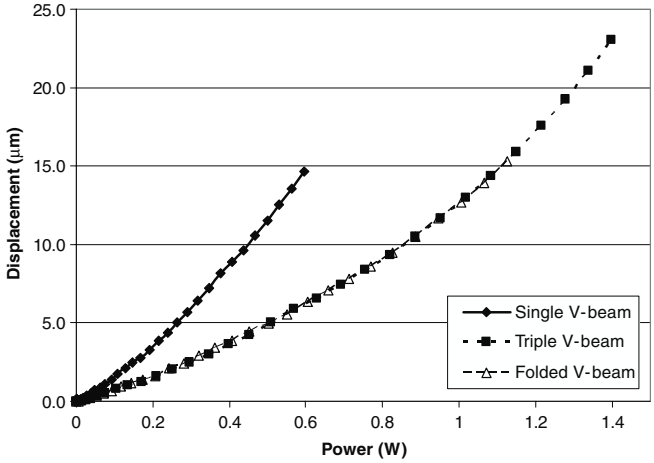


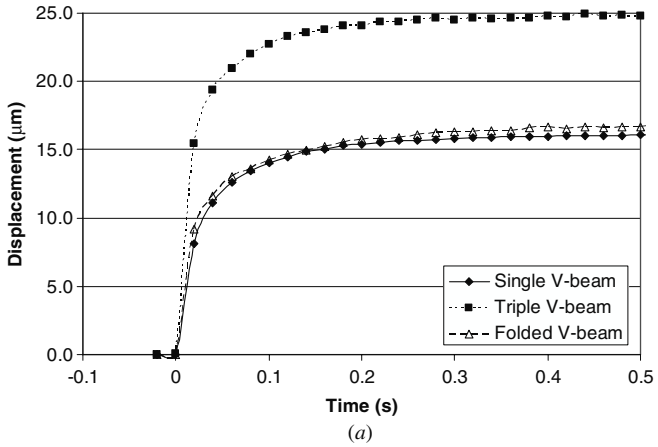
Figure 7. Experimental power-displacement curves including passive mechanism loading.

The transient analysis of the actuators is shown in figures 8(*a*) and (*b*), which show the measured step response and ring down behaviours, respectively.

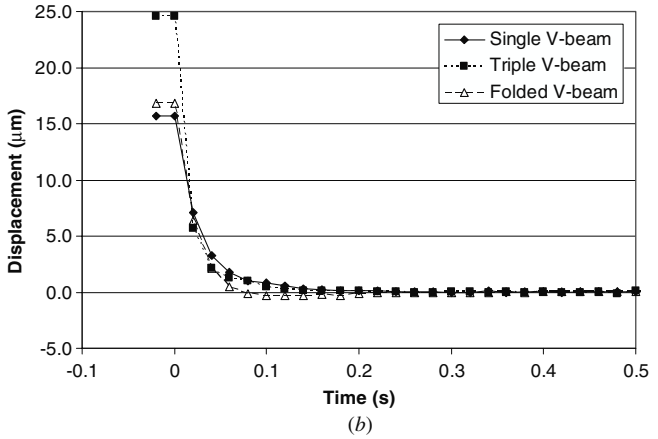
All three actuators required approximately the same time, approximately 0.4 s, to achieve their final position. The same held for the cooling down behaviour, in which the settling time was around 0.2 s for all actuators. The single V-beam concept and the triple V-beam concept had a similar cooling down behaviour, whereas the folded V-beam actuator showed a slight overshoot. The observed actuator behaviour is fast enough for most fibre alignment purposes.

5. Modelling results

Although the actual temperature in the beams could not be measured, experimental data about the electrical resistance and the deflection of the thermal actuators were available. These data are used to develop a finite element model for each actuator to determine the temperature distribution and the heat generation in the actuator beams. Furthermore, the



(*a*)



(*b*)

Figure 8. (*a*) Experimental step response and (*b*) ring down behaviour of the three different concepts at 34 V including passive mechanism loading.

models are used to make a complete comparison between the performances of the different actuators.

Comsol Multiphysics™ finite element modelling software was used to model the electrical, thermal and mechanical behaviour and their coupling. The model is further simplified by using only 2D geometries to significantly decrease calculation time. Also, the thin polysilicon resistor layer is not modelled separately. Instead, an equivalent electrical resistivity for the bulk silicon is calculated, which is considered admissible since the Biot number for the cross-section of the structures was very small [9]. This indicates that the internal cross-sectional temperature gradients are small and the required time for the heat to penetrate from the top of the cross-section to the bottom is short compared to the time required to transport the heat to the anchors.

The electrical resistivity is strongly dependent on temperature and differs depending on the doping type and level. With a phosphorous doping concentration of approximately 10^{20} atoms cm^{-3} in the polysilicon resistor layer, the equivalent electrical resistivity across the bulk silicon cross section was calculated to be 3.0×10^{-3} Ω m at room temperature. A linear expression for the electrical resistivity as a function of temperature is used to fit the modelled resistance to the measured values, which is adequate for these simulations. The thermal conductivity and the thermal

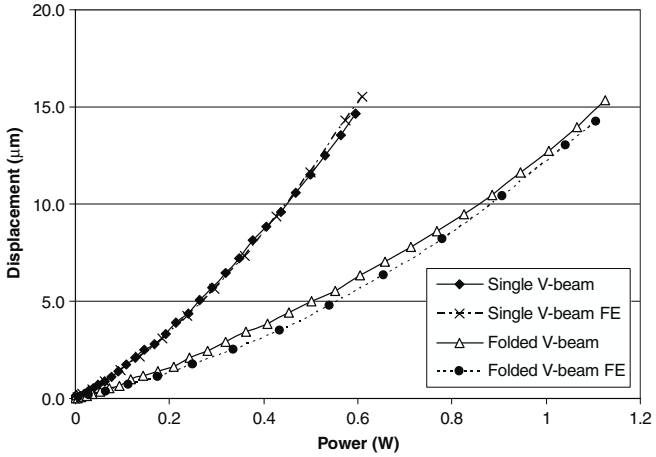


Figure 9. Experimental and modelled power-displacement curves of the single V-beam actuator and the folded V-beam actuator including passive mechanism.

expansion coefficient of single crystal silicon are also strongly temperature dependent and their values are taken from Lide [10] and Okada and Tokomaru [11], respectively.

In addition to heat conduction through the solid material, conductive and convective heat transfer through air and radiation are included. Temperature dependent values of density and thermal conductivity of air are taken from Mills [12], as well as formulae for the convection coefficient for macro systems, which are extrapolated to the micro domain. For the radiation estimation, the structures are modelled as grey bodies with an emissivity of 0.7 [9, 13].

The resistivity and displacement curves obtained by the model are in agreement with the experimental data and, therefore, the modelled temperatures are also assumed to be correct. The modelled displacement curves are shown together with the measured displacements in figure 9.

The modelled displacement matches the measured displacement within 5%. The exact amount of heat loss due to conduction through air at the top and bottom of the actuators could not be calculated since only 2D modelling was performed. Applying a larger convection coefficient compensated for this to approximate the right amount of heat loss.

The modelled temperature distribution of the improved folded V-beam actuator at 48 V is shown in figure 10.

To investigate the effect of the improvements on the temperature profile in the actuator, a second folded V-beam actuator is modelled using the FE software, only now without the reinforcements on the cold arms and with a smaller distance between the hot and cold arms. Similar to the original design by Syms *et al*, in this actuator the width of the restraining arms is the same as the width of the hot arms (in this case 25 μm), and the distance L_{hc} (see figure 1) between the cold and hot arms is decreased from 300 μm to 100 μm. Figure 11 shows the modelled temperature distribution of this folded V-beam actuator without the discussed geometrical improvements at 45 V input voltage, resulting in an approximately equal maximum temperature slightly above 770 K.

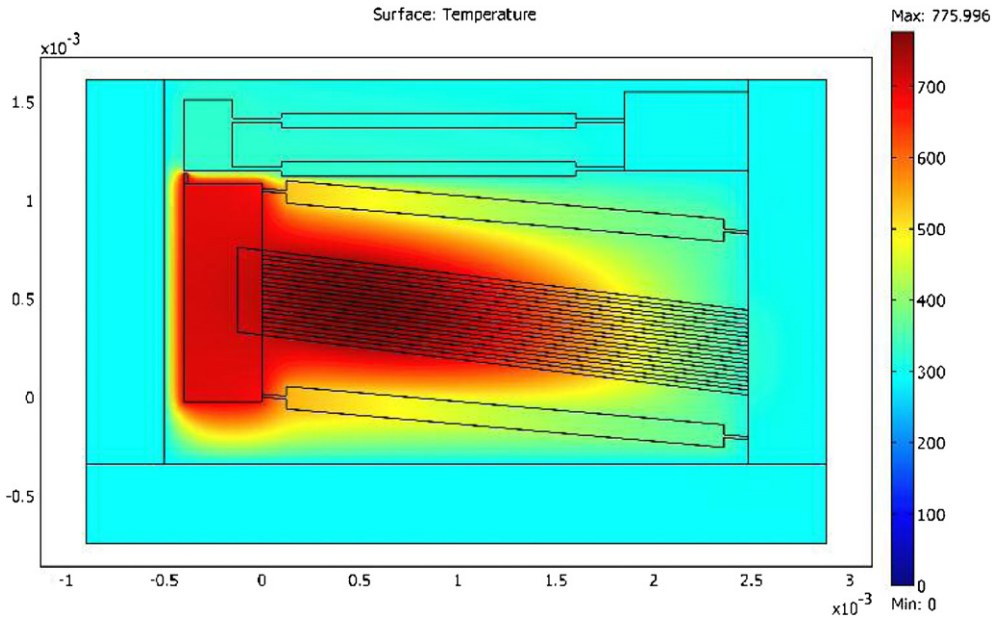


Figure 10. Modelled temperature distribution of the folded V-beam actuator with geometrical improvements at 48 V input voltage (in kelvin).

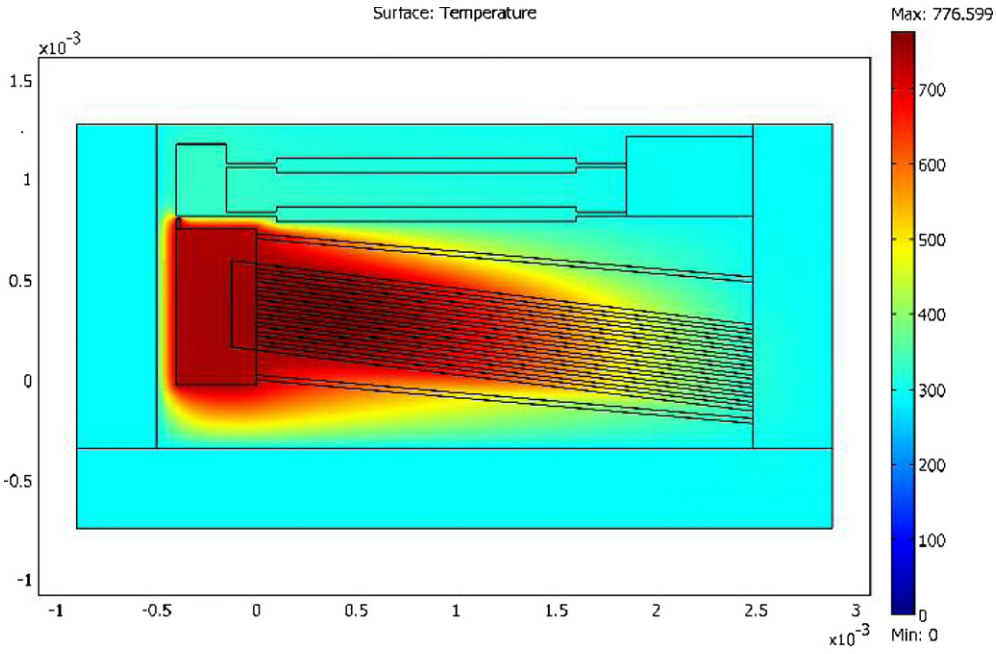


Figure 11. Modelled temperature distribution the folded V-beam actuator without geometrical improvements at 45 V input voltage (in kelvin).

The effect of the geometrical improvements on the temperature distribution can be seen from the differences in figures 10 and 11. It can be observed that for the improved actuator the highest temperature of 776 K is reached in the hot arms, instead of in the link bar as is the case for the design without the geometrical improvements. In addition, the restraining arms remained much cooler due to the larger distance to the hot arms and the increased heat-removing capacity of the reinforcements. This can also be seen in the temperature profiles along the restraining arms from the anchor to the link bar of both the improved folded V-beam actuator and the folded V-beam actuator without geometrical improvements shown in figure 12.

A lower temperature in the restraining arm results in smaller thermal expansion of this arm, improving the displacement performance of the actuator. As is clear from figure 12, the temperature in the restraining arm of the improved actuator is much lower towards the link bar. This can be attributed mainly to the geometry of the reinforced restraining arms. Although the narrow parts of the arms are narrower than the uniform arms used in the actuator without geometrical improvements (15 μm versus 25 μm), their overall thermal resistance combined with the reinforced

Table 1. Actuator performance comparison based on modelling results.

	V_{max} (V)	P (W)	u_{free} (μm)	F_{block} (mN)	A (mm^2)	W_{max} (nJ)	W_{max}/P (ns)	W_{max}/A (J m^{-2})
Single V-beam	44	0.95	35.5	39	6.2	680	720	0.110
Triple V-beam	38.5	1.79	38.5	36	3.6	690	380	0.191
Improved folded V-beam	48	1.94	43.0	48	4.7	1030	530	0.219
Folded V-beam without geometrical improvements	45	1.72	26.9	20	3.3	270	160	0.084

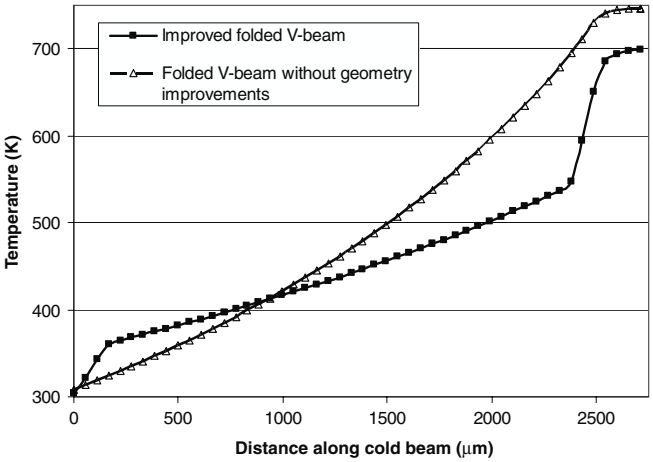


Figure 12. Modelled temperature profile along the length of the restraining arm of the improved folded V-beam actuator and the folded V-beam actuator without geometrical improvements (from the substrate anchor on the left to the link bar on the right).

parts is smaller. Heat passing from the link bar into the arm first encounters a high thermal resistance after which it can flow much more easily when reaching the reinforced part, resulting in a large temperature drop over the narrow segment attached to the link bar. Combined with a larger distance L_{hc} and the smaller overall thermal resistance, this results in a significantly lower average restraining arm temperature, at only a small reduction in actuator efficiency.

6. Performance comparison

A performance comparison between the improved folded V-beam actuator and the two other fabricated configurations is performed by means of calculations made on the output work. The maximum possible output work that can be produced by an actuator is given by equation (1):

$$W_{max} = \tfrac{1}{2}ku_{free}^2 = \tfrac{1}{2}F_{block}u_{free}. \quad (1)$$

Here, the actuator stiffness k equals the blocking force F_{block} divided by the free actuator displacement u_{free}. In practice, the actual output work is lower for different types of actuator loading. For instance, in the case of a constant load or a spring load on the actuator, the output work is only 1/2 and 1/4, respectively, of the maximum possible output work. The performance of an actuator is typically described in terms of the work per actuator volume or the work per unit of input power. These are measures of the actuator effectiveness and efficiency, respectively. For the actuator configurations at hand, the work per actuator volume ratio is considered less suitable because it only includes the active actuator volume, whereas all concepts required additional structures or substrate parts to work properly. Therefore, instead, the ratio work per required chip area W_{max}/A is used, which does include the extra structures and substrate parts, and which can be considered an important practical performance criterion for designers, as indicated in the introduction.

Table 1 shows the results of the calculations made for each actuator concept, which are based on the FE modelling results. The power and work are calculated for the voltage levels at which the actuator temperatures reach the maximum value of 770 K. For comparison, the modelled performance of the folded V-beam actuator without geometrical improvements introduced in the previous section is also included. The required chip area for the two V-beam concepts with an additional lever also included the part of the substrate required to hold the anchors in place. The folded V-beam actuators had their anchors at one side and therefore the surrounding substrate was not included in the chip area. The surrounding air, however, was included because it functions as isolation buffer to prevent heat loss towards the substrate.

The improved folded V-beam actuator required the largest amount of power to reach the maximum temperature. However, both the free displacement and blocking force are also the largest. Therefore, its maximum delivered work is by far the highest of all three fabricated actuators. It is also the most effective with respect to area by 15%, because the required chip area is quite comparable to the other concepts. Due to the larger required power, the efficiency, denoted by W_{max}/P, is lower than for the concept with the single V-beam actuator, having the highest efficiency. This concept used the largest chip area and, therefore, it is least effective with respect to area of the three fabricated actuators.

When comparing the improved folded V-beam actuator with the folded V-beam actuator without geometrical improvements, it can be observed that the addition of the reinforcements and the larger distance between the hot and cold arms resulted in over a twofold increase of the work per area ratio at just a small rise of required input power. Compared to the original design presented by Syms *et al* [5], on the basis of data available in the paper, even an estimated five times work per area increase is achieved, at less than a third of the required input power.

Syms *et al* observed that decreasing the width of the uniform restraining arms increased the unloaded actuator displacement. However, with narrower restriction arms the stiffness in the longitudinal direction is decreased. This

decreases their restraining capabilities and consequently the performance under load is lowered. On the other hand, widening the arms also results in lower performance due to a higher rigidity and increased heat leakage. Compared to restraining arms having a uniform width, the reinforced cold arms in the improved design perform very well because they increase the longitudinal stiffness without affecting the lateral stiffness.

The folded V-beam concept has many dimensions that can be modified and thus many geometrical variations are possible. Further optimization of the actuator is still considered feasible. For instance, the optimal angle difference between hot and cold arms was determined to be smaller than the chosen 2°. Tests on a concept with an angle difference of 1.5° showed a somewhat larger deflection at the same voltage and power levels. All three actuator concepts are scalable in a similar manner to achieve modified actuation strokes and blocking forces. Scaling of the concepts, therefore, is not expected to result in different comparison results.

7. Conclusion

The paper presents an improved folded V-beam actuator design for single-ended in-plane thermal fibre alignment, allowing clear access to the fibre tip. In addition to modifications on the fabrication, improvements on the geometry are made. By reinforcing the cold restraining arms and by placing them further away from the hot actuator arms, both the mechanical and the thermal performance are improved. The actuator performance is compared to two other actuator configurations, both consisting of a well-known V-beam actuator in combination with a lever to obtain the same clear fibre tip access. A complete range of measurements is performed to investigate the steady-state and transient behaviour of the individual concepts. Performance comparisons have shown that the improved folded V-beam actuator delivers 15% more work per area and is therefore considered an attractive alternative solution for optical fibre alignment.

Acknowledgments

This research is part of the Delft Centre for Mechatronics and Microsystems of the Delft University of Technology. It is funded by the Dutch government programme IOP Precision Engineering as part of the project IPT02310 Technologies for in-package optical fibre chip coupling. Many thanks are due to the DIMES IC Processing group and particularly to Wim van der Vlist for the device processing.

References

[1] Guckel H, Klein J, Christenson T, Skrobis K, Laudon M and Lovell E 1992 Thermo-magnetic metal flexure actuators *Tech. Dig. 5th IEEE Solid-State Sensors and Actuators Workshop (Hilton Head, USA, June 22–25)* pp 73–5

[2] Comtois J H, Bright V M and Phipps M W 1995 Thermal microactuators for surface-micromachining processes *Proc. SPIE* **2642** 10–21

[3] Kopka P, Hoffmann M and Voges E 2000 Coupled cantilever actuators for 1×4 and 2×2 optical switches *J. Micromech. Microeng.* **10** 260–4

[4] Que L, Park J-S, Li M-H and Gianchandani Y B 2000 Reliability studies of bent-beam electro-thermal actuators *Proc. 38th IEEE Int. Reliability Physics Symp. (San Jose, USA)* pp 118–22

[5] Syms R R A, Zou H, Yao J, Uttamchandani D and Stagg J 2004 Scalable electrothermal MEMS actuator for optical fibre alignment *J. Micromech. Microeng.* **14** 667–74

[6] Veladi H, Syms R R A and Zou H 2007 Fiber-pigtailed electrothermal MEMS iris VOA *IEEE J. Lightw. Technol.* **25** 2159–62

[7] Ehmann M, Ruther P, von Arx M and Paul O 2001 Operation and short-term drift of polysilicon-heated CMOS microstructures at temperatures up to 1200 K *J. Micromech. Microeng.* **11** 397–401

[8] Lee J, Beechem T, Wright T L, Nelson B A, Graham S and King W P 2006 Electrical, thermal, and mechanical characterization of silicon microcantilever heaters *J. Microelectromech. Syst.* **15** 1644–55

[9] Hickey R, Sameoto D, Hubbard T and Kujath M 2003 Time and frequency response of two-arm micromachined thermal actuators *J. Micromech. Microeng.* **13** 40–6

[10] Lide D R 2006 *Handbook of Chemistry and Physics* 87th edn (Boca Raton, FL: CRC Press)

[11] Okada Y and Tokomaru Y 1984 Precise determination of lattice parameter and thermal expansion coefficient of silicon between 300 and 1500 K *J. Appl. Phys.* **56** 314–20

[12] Mills A F 1999 *Basic Heat and Mass Transfer* 2nd edn (Upper Saddle River, NJ: Prentice-Hall)

[13] Mankame N D and Ananthasuresh G K 2001 Comprehensive thermal modeling and characterization of an electro-thermal-compliant microactuator *J. Micromech. Microeng.* **11** 452–62